Wide-Field Interferometric Imaging: A Powerful Tool for the Terrestrial Planet Finder

S. A. Rinehart[1,2], D. Leisawitz[1], B. Frey[1], M. Kuchner[3], D. Leviton[1], L. Lobsinger[1], A. Martino[1], & L. Mundy[4]

1: NASA – GSFC 2: National Research Council 3: Princeton Univ. 4: Univ. of Maryland

Abstract

We present a discussion of the design and construction of the Wide-Field Imaging Interferometry Testbed (WIIT) at the Goddard Space Flight Center. The testbed is motivated by a need to develop techniques for wide-field interferometric imaging in the optical/IR for future space missions such as TPF. Theoretically, using multipixel detectors for spatial multiplexing/mosaicing allows this, but in practice there are a number of questions which WIIT will address. We present some initial data acquired with this system and demonstrate its capability to produce wide-field interferometry data.

Motivation

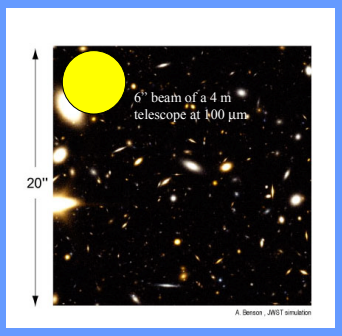

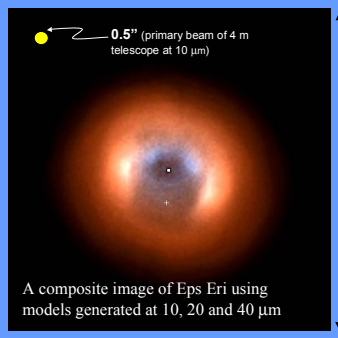

"To ensure a broad science return from TPF, the committee recommends that, in planning the mission, comparable weight be given to the two broad science goals: studying planetary systems and studying the structure of astronomical sources at infrared wavelengths." (from the Decadal Report). The Wide-Field Imaging Interferometry Testbed was originally conceived to develop techniques and tools necessary for wide field-of-view interferometric imaging with FIR/Sub-mm missions such as SPECS (Submillimeter Probe of the Evolution of Cosmic Structure). For extragalactic surveys and studies of star formation regions, the small FOV inherent to Michelson stellar interferometers is insufficient, so techniques for wide FOVs are necessary. Similarly, in order to image star formation regions, debris disks, and to explore Origins themes, an interferometric TPF requires wide FOV techniques. The figure at the above right shows a model of the Eps Eri debris disk (the planet is marked by the + sign). In order to image the disk using an interferometric TPF (with 4-m telescopes) would require over 400 separate pointings! Using the techniques being explored with WIIT, the FOV could be enlarged by a areal factor of over 10000, thereby allowing observation of such a debris disk in a single pointing.

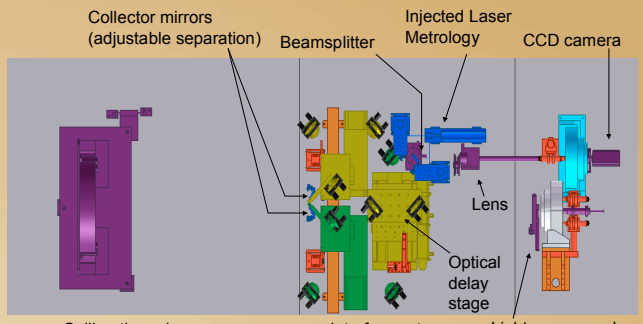

Layout of the Wide-Field Imaging Interferetry Testbed (WIIT). The testbed is designed to provide proof-of-concept of wide-field imaging interferometry. The source (on right) illuminates the collimator. The collimated beam returns to the two collector mirrors, and travels through a series of flat mirrors to the beam combiner. One of the two output ports of the interferometer continues to the science camera. To provide optical delay, one of the two arms of the interferometer uses a high-precision linear stage with two flat mirrors in a rooftop configuration. Full u-v plane coverage is provided by adjusting the baseline length and rotating the source scene.

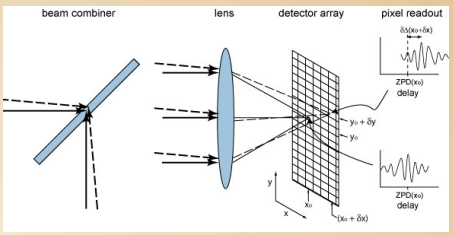

The principle of wide-field imaging is relatively straightforward. A source on the sky appears on a pixel (x_o, y_o), and as the delay line scans through Zero Path Difference (ZPD), the series of images produce an interferogram on the pixel in the time domain. For a second source separated by some angular offset, the image appears on a pixel ($x_o + \delta x$, y_o), where $\delta x = f_{lens}\theta$. The delay line scan produces an interferogram here as well, but with a shift in the ZPD of the interferogram.

Testbed Performance

Table 1: Sources of Visibility Loss in WIIT

Source	Parameter Specification: Design Spec	Achieved	Formula	Visibility: Value
Alignment				
Coalignment at Pupil Plane	>95% overlap	97.5%	$1-\eta$	0.975
Tip/Tilt at Exit Pupil	<0.5 arcsec	0.5 arcsec	$\frac{\Delta\lambda/\lambda\pi\Delta\theta/\lambda}{\lambda\pi\Delta/\lambda}$	(0.988) [a]
Optics				
Collimating Mirror				
Surface roughness	15.75 nm		$e^{-(4\pi\delta/\lambda)^2}$	(0.98) [a]
Beamsplitter				
Surface roughness	15 nm		$e^{-(4\pi\delta/\lambda)^2}$	(0.98) [a]
Interferometer Mirrors				
Surface roughness	10 nm		$e^{-(4\pi\delta/\lambda)^2}$	(0.92) [a]
Combined observed effect (Optics & Tilt)				0.93
Intensity Mismatch	>80% match	80%	$2/(g^{1/2}+g^{-1/2})$	0.994
Positional Knowledge	20 nm	9.89 nm	NC[b]	0.998
Frame Exposure Time	<20 ms	<10 ms	NC[b]	0.99966
Total Predicted Visibility				0.985

Table 2: Sources of Visibility Uncertainty in WIIT

Source	Parameter	Value	Formula	Uncertainty at (I_{max})	Uncertainty at (I_{min})
Camera					
Bit Noise	a_{bit}	0.5	a_{bit}/N_{max}	0.0083	0.025
Photon Counting	N_{noise}	10000	$\sqrt{2(N_{max})+(2^q/N_{max})}$	0.0185	0.0253
Camera noise (read noise, dark current)	a_{det}	0.66	$2a_{det}/N_{max}$	0.0088	0.0165
Turbulence					
Wavefront distortion	Measured			0.05[c]	0.05[c]
Total Uncertainty in Measured Visibility					
Single Pixel					0.111
2x2 pixels					0.078

Tablenotes:
a: Parentheses indicate that this parameter is rolled into measured values.
b: NC indicates a numerically calculated quantity.
c: Estimated values based on preliminary data.

The tables above enumerate the sources of visibility loss in WIIT and sources of uncertainty in measured visibilities. The dominant effect in both cases is distortion of the wavefront due to optical surface errors and turbulent effects. Because WIIT operates at visible wavelengths in atmosphere, these effects are not comparable to sources of uncertainty in future interferometric space missions.

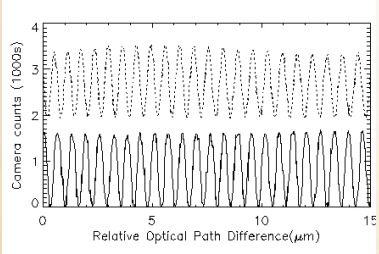

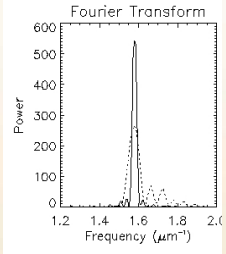

The plot on the far left shows laser fringes acquired by WIIT with open-loop (dotted) and closed-loop (solid) metrology. The improvement provided by closed loop metrology is clear, especially in the Fourier transform of the fringes in the plot on the near left.

Demonstration of Wide Field-of-View

These figures demonstrate wide FOV interferometric imaging. At right is a picture of the source. Lower right is a schematic of the profiles of the two vertical lines, and at lower left are the eight interferograms produced by 8 pixels spanning the two lines. We clearly see the shift in ZPD of the fringes for the two lines, and the blending of the interferograms where the beam profiles overlap.

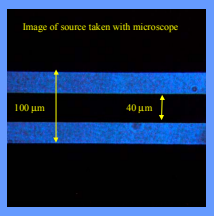

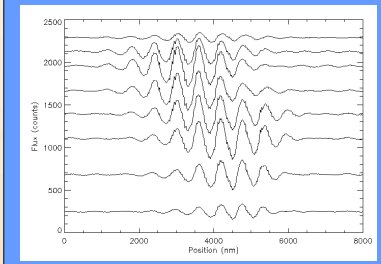

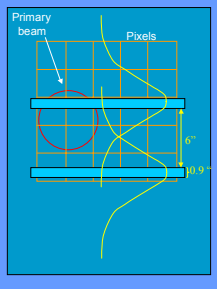

This series of three plots show the results of some of our early data from observing a 20 μm pinhole with no bandpass filter. The data are in good agreement with predictions. Ongoing efforts are expected to improve the overall data quality significantly.

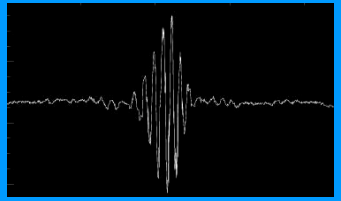

An observed white light interferogram from WIIT.

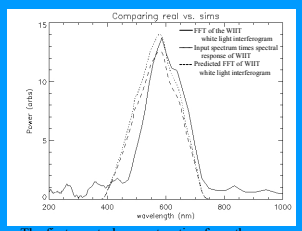

The first spectral reconstruction from the observed white-light interferogram.

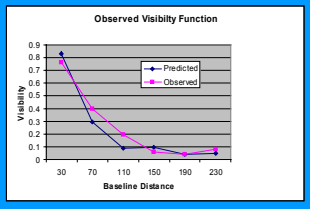

A measured visibility function compared against the predicted function.

References:

Leisawitz, et al. Wide-field imaging interferometry testbed I: purpose, testbed design, data, and synthesis algorithms. Proc. SPIE, 4852, 255, 2003.

Leviton, et al. Wide-field imaging interferometry testbed III: metrology subsystem. Proc. SPIE, 4852, 827 , 2003.

Rinehart, et al. Wide-field imaging interferometry testbed II: implementation, performance, and plans . Proc. SPIE, 4852, 674, 2003.

Astronomy and Astrophysics in the New Millenium, National Academies Press, Washington, DC, 2001 (Decadal Report).

Acknowledgements:

The authors would like to thank Sean Moran, who's thesis work produced the models of Eps Eri. S. Rinehart is supported as a Resident Research Associate at NASA – GSFC by the National Research Council. The authors would also like to thank members of the Science and Technical Advisory Group (STAG) for continued advice and assistance. Development of the Wide-field Imaging Interferometry Testbed was funded by NASA through the ROSS/SARA program.